Condensed Matter Physics, 2015, Vol. 18, No 4, 43703: 1–16
DOI: 10.5488/CMP.18.43703
http://www.icmp.lviv.ua/journal

arXiv:1512.07799v1 [cond-mat.mtrl-sci] 24 Dec 2015

Statistical theory of thermodynamic and dynamic properties of the $RbHSO_4$ ferroelectrics

I.R. Zachek[1], R.R. Levitskii[2], Ya.Shchur[2], O.B.Bilenka[1]

[1] Lviv Polytechnic National University, 12 Bandera St., 79013 Lviv, Ukraine

[2] Institute for Condensed Matter Physics of the National Academy of Sciences of Ukraine, 1 Svientsitskii St., 79011 Lviv, Ukraine

Received June 10, 2015, in final form August 5, 2015

Within the modified four-sublattice model of $RbHSO_4$ with taking into account the piezoelectric coupling to the strains ε_i, ε_4, ε_5, and ε_6, the polarization components, static and dynamic dielectric permittivity of clamped and free crystal are calculated in the mean field approximation. At the proper choice of the values of the theory parameters, a satisfactory quantitative description of the available experimental data is obtained.

Key words: *ferroelectric, dielectric permittivity, piezomodule*

PACS: *77.22.Ch, 77.22.Gm, 77.65.-j, 77.80.Bh, 77.84.-s*

1. Introduction

Chemical compounds such as sodium-potassium tartrate $NaKC_4H_4O_6{\cdot}4H_2O$ (Rs), sodium-ammonium tartrate $NaNH_4C_4H_4O_6{\cdot}4H_2O$ (ARs), rubidium hydrosulphate $RbHSO_4$ (RHS), and ammonium hydrosulphate NH_4HSO_4 (AHS) belong to the order-disorder type ferroelectrics. According to neutron and X-ray structure studies of RHS [1–4], Rb^{87} [5] and D^2 [6, 7] NMR measurements, infrared [8] and Raman scattering experiments [9], the phase transition in RHS is of the second order. Protons are already ordered in the paraelectric phase. Only one second-order phase transition point (T_c = 265 K) is present. In the high-temperature phase, the structure of RHS is monoclinic and is described by the space group $P2_1/c$–C^5_{2h}. Below the transition point, the monoclinic symmetry remains, but the space group changes to Pc–C^2_s. The unit cell consists of eight molecules $Z = 8$ in both phases.

The phase transition in RHS is associated with the motion of sulphate complexes $(SO_4)_{11}$, $(SO_4)_{12}$, $(SO_4)_{13}$, $(SO_4)_{14}$ between two equilibrium positions. $(SO_4)_{25}$, $(SO_4)_{26}$, $(SO_4)_{27}$, $(SO_4)_{28}$-complexes are completely ordered in the entire temperature range and do not play any direct role in the ferroelectric phase transition. These complexes form a network of elementary dipoles directed along the z-axis (figure 1).

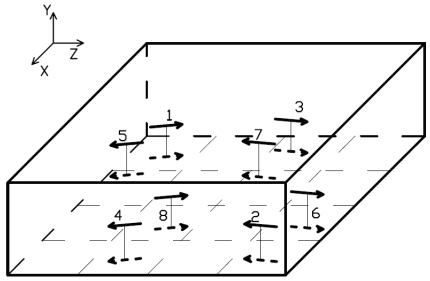

Figure 1. Orientations of the $\mathbf{d}_{qf}$ vectors within the primitive cell of R_s in the high-symmetry phase (the paraelectric phase).

© I.R. Zachek, R.R. Levitskii, Ya.Shchur, O.B.Bilenka, 2015

The dipole moments created in the paraelectric phase by the (14) and (12) (SO_4) complexes have the same direction which is opposite to the direction of the dipole moments created by the (11) and (13) complexes. Analogously, the dipole moments of the (25) and (26) type complexes are opposite to those of the (27) and (28) complexes.

Two equilibrium positions (potential wells) of the $(1f)$-complexes ($f = 1,2,3,4$) are not equivalent. Above the transition temperature T_c, the $(1f)$-complexes are located in the energetically favorable equilibrium positions (deeper potential wells). Mathematically, non-equivalence of equilibrium positions is described by an additional longitudinal field Δ acting on the dipoles of the sulphate-complexes. This field is oppositely directed for the (11), (14) and (12) complexes.

The phenomenological [10] and statistic [11–15] models of the phase transition in RHS-crystals, analogously to the Mitsui model for Rs, well describe the dielectric properties [16–20] and the Debye-type dynamic dielectric permittivity [12–15] in the mean field approximation. However, it is impossible to calculate the experimentally measurable dielectric permittivity of a mechanically free crystal, the piezoelectric coefficients, elastic constants and transverse dielectric permittivities using these models [12–15]. That is why the piezoelectric coupling to the strains should be taken into account [21].

In this work we propose a modification of the four-sublattice model of the $RbHSO_4$ crystals, which takes into account the piezoelectric coupling to the strains $\varepsilon_i, \varepsilon_j$ in the ferroelectric phase. The dielectric, piezoelectric, elastic, thermal and dynamic characteristics of RHS are calculated within the mean field approximation. The corresponding experimental data for this crystal are described.

2. Four-sublattice model: Hamiltonian

The system Hamiltonian is a modification of the Hamiltonian proposed in [22] that takes into account the piezoelectric coupling, and a generalization of the Hamiltonian in [13] to the 'three-dimensional' model. In the quasi-spin representation, it reads as follows:

$$\begin{aligned}\hat{H} &= NU_{\text{seed}} - \frac{1}{2}\sum_{qq'}\sum_{f=1}^{4} J_{ff}(qq')\frac{\sigma_{qf}}{2}\frac{\sigma_{q'f}}{2} - \frac{1}{2}\sum_{qq'}\sum_{f\neq f'} K_{ff'}(qq')\frac{\sigma_{qf}}{2}\frac{\sigma_{q'f'}}{2} \\ &\quad -\Delta\sum_{q}\Big(-\frac{\sigma_{q1}}{2}-\frac{\sigma_{q2}}{2}+\frac{\sigma_{q3}}{2}+\frac{\sigma_{q4}}{2}\Big) - \mu_1 E_1\sum_{q}\Big(\frac{\sigma_{q1}}{2}-\frac{\sigma_{q2}}{2}+\frac{\sigma_{q3}}{2}-\frac{\sigma_{q4}}{2}\Big) \\ &\quad -\mu_2 E_2\sum_{q}\Big(-\frac{\sigma_{q1}}{2}+\frac{\sigma_{q2}}{2}+\frac{\sigma_{q3}}{2}-\frac{\sigma_{q4}}{2}\Big) - \mu_3 E_3\sum_{q}\Big(\frac{\sigma_{q1}}{2}+\frac{\sigma_{q2}}{2}+\frac{\sigma_{q3}}{2}+\frac{\sigma_{q4}}{2}\Big),\end{aligned} \tag{2.1}$$

where N is the number of unit cells. In (2.1) $J_{ff'}(qq')$ and $K_{ff'}(qq')$ are the interaction potentials between the pseudospins from the same and from different chains, respectively; the parameter Δ describes the asymmetry of the potential, in which the pseudospins move; μ_i is the effective dipole moment per one pseudospin; σ_{qf} is the z-component of the pseudospin operator situated at f-th bond ($f = 1,2,3,4$) in q-th unit cell.

$U_{1\text{seed}}$ is the seed energy that includes the elastic, piezoelectric and dielectric contributions expressed in terms of the electric fields E_i ($i = 1,2,3$) and strains ε_i and ε_j ($j = i+3$). $c_{jj}^{E0}(T)$, e_{ij}^0, $\chi_{ii}^{\varepsilon 0}$ are the so-called seed elastic and piezoelectric constants and dielectric permittivities:

$$\begin{aligned}U_{\text{seed}} &= v\Big[\frac{1}{2}\sum_{i,i'=1}^{3} c_{ii'}^{E0}(T)\varepsilon_i\varepsilon_{i'} + \frac{1}{2}\sum_{j=4}^{6} c_{jj}^{E0}(T)\varepsilon_j^2 - \sum_{i=1}^{3} e_{3i}^0\varepsilon_i E_3 - e_{35}^0\varepsilon_5 E_3 \\ &\quad -\frac{1}{2}\chi_{11}^{\varepsilon 0}E_1^2 - \frac{1}{2}\chi_{22}^{\varepsilon 0}E_2^2 - \frac{1}{2}\chi_{33}^{\varepsilon 0}E_3^2\Big],\end{aligned} \tag{2.2}$$

v is the unit cell volume.

Having analyzed the results of [23], we assume the seed elastic constants $c_{jj}^{E0}(T)$ to be linearly decreasing with temperature [24]

$$c_{ii'}^{E0}(T) = c_{ii'}^{E0} - k_{ii'}(T - T_c), \qquad c_{jj}^{E0}(T) = c_{jj}^{E0} - k_{jj}(T - T_c), \tag{2.3}$$

where the coefficients k_{jj} phenomenologically take into account the high-temperature lattice anharmonism.

We make an identity transformation

$$\sigma_{qf} = \eta_f + (\sigma_{qf} - \eta_f), \qquad (f = 1,2,3,4), \tag{2.4}$$

and neglect the quadric fluctuations. The Fourier transforms of the interaction constants at $\mathbf{q} = 0$, $J = J_{ff} = \sum_{q'} J_{ff}(qq')$, $K_{ff'} = \sum_{q'} K_{ff'}(qq')$ and Δ are expanded in series over the strains ε_i, ε_j up to the linear terms:

$$\begin{aligned}
&J = J^0 + \frac{\partial J}{\partial \varepsilon_i}\varepsilon_i = J^0 + \sum_{i=1}^{3}\psi_{1i}\varepsilon_i + \sum_{j=4}^{6}\psi_{1j}\varepsilon_j, && K_{12} = K_{12}^0 + \sum_{i=1}^{3}\psi_{2i}\varepsilon_i + \sum_{j=4}^{6}\psi_{2j}\varepsilon_j,\\
&K_{13} = K_{13}^0 + \sum_{i=1}^{3}\psi_{3i}\varepsilon_i + \sum_{j=4}^{6}\psi_{3j}\varepsilon_j, && K_{14} = K_{14}^0 + \sum_{i=1}^{3}\psi_{4i}\varepsilon_i + \sum_{j=4}^{6}\psi_{4j}\varepsilon_j,\\
&\Delta = \Delta^0 + \sum_{i=1}^{3}\psi_{5i}\varepsilon_i + \sum_{j=4}^{6}\psi_{5j}\varepsilon_j.
\end{aligned} \tag{2.5}$$

As a result, Hamiltonian (2.1) within the mean field approximation takes the form:

$$\begin{aligned}
H^{(0)} &= \nu U_{\text{seed}} + \frac{1}{8}J^0\left(\eta_1^2+\eta_2^2+\eta_3^2+\eta_4^2\right)\\
&+\frac{1}{4}K_{12}^0\left(\eta_1\eta_2+\eta_3\eta_4\right)+\frac{1}{4}K_{13}^0\left(\eta_1\eta_3+\eta_2\eta_4\right)+\frac{1}{4}K_{14}^0\left(\eta_1\eta_4+\eta_2\eta_3\right)\\
&+\frac{1}{8}\Big(\sum_{i=1}^{3}\psi_{1i}\varepsilon_i+\sum_{j=4}^{6}\psi_{1j}\varepsilon_j\Big)\left(\eta_1^2+\eta_2^2+\eta_3^2+\eta_4^2\right)+\frac{1}{4}\Big(\sum_{i=1}^{3}\psi_{2i}\varepsilon_i+\sum_{j=4}^{6}\psi_{2j}\varepsilon_j\Big)\left(\eta_1\eta_2+\eta_3\eta_4\right)\\
&+\frac{1}{4}\Big(\sum_{i=1}^{3}\psi_{3i}\varepsilon_i+\sum_{j=4}^{6}\psi_{3j}\varepsilon_j\Big)\left(\eta_1\eta_3+\eta_2\eta_4\right)+\frac{1}{4}\Big(\sum_{i=1}^{3}\psi_{4i}\varepsilon_i+\sum_{j=4}^{6}\psi_{4j}\varepsilon_j\Big)\left(\eta_1\eta_4+\eta_2\eta_3\right),
\end{aligned} \tag{2.6}$$

$$\hat{H}_s = -\sum_q\left(\mathscr{H}_1\frac{\sigma_{q1}}{2}+\mathscr{H}_2\frac{\sigma_{q2}}{2}+\mathscr{H}_3\frac{\sigma_{q3}}{2}+\mathscr{H}_4\frac{\sigma_{q4}}{2}\right). \tag{2.7}$$

Thus, we find the mean pseudospin values

$$\eta_f = \tanh\frac{\beta}{2}\mathscr{H}_f. \tag{2.8}$$

Let us use new variables:

$$\begin{aligned}
\xi_1 &= \frac{1}{4}(-\eta_1-\eta_2+\eta_3+\eta_4) = \frac{1}{4}\left(-\tanh\frac{\beta}{2}\mathscr{H}_1-\tanh\frac{\beta}{2}\mathscr{H}_2+\tanh\frac{\beta}{2}\mathscr{H}_3+\tanh\frac{\beta}{2}\mathscr{H}_4\right),\\
\xi_2 &= \frac{1}{4}(-\eta_1+\eta_2+\eta_3-\eta_4) = \frac{1}{4}\left(-\tanh\frac{\beta}{2}\mathscr{H}_1+\tanh\frac{\beta}{2}\mathscr{H}_2+\tanh\frac{\beta}{2}\mathscr{H}_3-\tanh\frac{\beta}{2}\mathscr{H}_4\right),\\
\xi_3 &= \frac{1}{4}(\eta_1+\eta_2+\eta_3+\eta_4) = \frac{1}{4}\left(\tanh\frac{\beta}{2}\mathscr{H}_1+\tanh\frac{\beta}{2}\mathscr{H}_2+\tanh\frac{\beta}{2}\mathscr{H}_3+\tanh\frac{\beta}{2}\mathscr{H}_4\right),\\
\zeta &= \frac{1}{4}(\eta_1-\eta_2+\eta_3-\eta_4) = \frac{1}{4}\left(\tanh\frac{\beta}{2}\mathscr{H}_1-\tanh\frac{\beta}{2}\mathscr{H}_2+\tanh\frac{\beta}{2}\mathscr{H}_3-\tanh\frac{\beta}{2}\mathscr{H}_4\right),
\end{aligned} \tag{2.9}$$

where the self-consistency fields $\mathscr{H}_f$ are given by the expressions:

$$\begin{aligned}
&\mathscr{H}_1 = (-\gamma_1-\gamma_2+\gamma_3+\delta), && \mathscr{H}_2 = (-\gamma_1+\gamma_2+\gamma_3-\delta),\\
&\mathscr{H}_3 = (\gamma_1+\gamma_2+\gamma_3+\delta), && \mathscr{H}_4 = (\gamma_1-\gamma_2+\gamma_3-\delta),
\end{aligned} \tag{2.10}$$

and

$$\gamma_1 = \left(\frac{J_1}{2}\xi_1+\mu_1E_1\right), \quad \gamma_2 = \left(\frac{J_2}{2}\xi_2+\mu_2E_2\right), \quad \gamma_3 = \left(\frac{J_3}{2}\xi_3+\mu_3E_3\right), \quad \delta = \left(\frac{J_4}{2}\zeta+\Delta\right).$$

Taking into account (2.3), we obtain

$$J_1 = J_1^0 + \sum_{i=1}^{3} \bar{\psi}_{1i}\varepsilon_i + \sum_{j=4}^{6} \bar{\psi}_{1j}\varepsilon_j, \qquad J_2 = J_2^0 + \sum_{i=1}^{3} \bar{\psi}_{2i}\varepsilon_i + \sum_{j=4}^{6} \bar{\psi}_{2j}\varepsilon_j,$$
$$J_3 = J_3^0 + \sum_{i=1}^{3} \bar{\psi}_{3i}\varepsilon_i + \sum_{j=4}^{6} \bar{\psi}_{3j}\varepsilon_j, \qquad J_4 = J_4^0 + \sum_{i=1}^{3} \bar{\psi}_{4i}\varepsilon_i + \sum_{j=4}^{6} \bar{\psi}_{4j}\varepsilon_j,$$
$$\Delta = \Delta^0 + \sum_{i=1}^{3} \psi_{5i}\varepsilon_i + \sum_{j=4}^{6} \psi_{5j}\varepsilon_j, \tag{2.11}$$

where

$$J_1^0 = -J^0 - K_{12}^0 + K_{13}^0 + K_{14}^0, \qquad J_2^0 = J^0 - K_{12}^0 - K_{13}^0 + K_{14}^0,$$
$$J_3^0 = J^0 + K_{12}^0 + K_{13}^0 + K_{14}^0, \qquad J_4^0 = J^0 - K_{12}^0 + K_{13}^0 - K_{14}^0, \tag{2.12}$$

$$\bar{\psi}_{1i} = -\psi_{1i} - \psi_{2i} + \psi_{3i} + \psi_{4i}, \qquad \bar{\psi}_{1j} = -\psi_{1j} - \psi_{2j} + \psi_{3j} + \psi_{4j},$$
$$\bar{\psi}_{2i} = \psi_{1i} - \psi_{2i} - \psi_{3i} + \psi_{4i}, \qquad \bar{\psi}_{2j} = \psi_{1j} - \psi_{2j} - \psi_{3j} + \psi_{4j},$$
$$\bar{\psi}_{3i} = \psi_{1i} + \psi_{2i} + \psi_{3i} + \psi_{4i}, \qquad \bar{\psi}_{35} = \psi_{15} + \psi_{25} + \psi_{35} + \psi_{45},$$
$$\bar{\psi}_{4i} = \psi_{1i} - \psi_{2i} + \psi_{3i} - \psi_{4i}, \qquad \bar{\psi}_{45} = \psi_{15} - \psi_{25} + \psi_{35} - \psi_{45}.$$

Parameters ξ_1, ξ_2, ξ_3 describe the dipole pseudospin ordering along the a, b and c-axes, respectively, and the parameter ζ is responsible for the paraelectric phase pseudospin ordering.

Without external electric fields and mechanical strains, the pseudospin mean values in the paraelectric phases are $\eta_1 = -\eta_2 = \eta_3 = -\eta_4 = \eta$ and $\xi_{1p} = \xi_{2p} = \xi_{3p} = 0$, respectively, and

$$\zeta_p = \tanh\frac{\beta}{2}\left(\frac{J_4}{2}\zeta_p + \Delta\right). \tag{2.13}$$

In the ferroelectric phase at zero fields $E_i = 0$ and stresses $\sigma_j = 0$, $\eta_1 = \eta_3 = \eta_{13}$, $\eta_2 = \eta_4 = \eta_{24}$. As a result $\xi_{1s} = 0$, $\xi_{2s} = 0$, and

$$\xi_{3s} = \frac{1}{2}\left[\tanh\frac{\beta}{2}\left(\frac{J_3}{2}\xi_{1s} + \frac{J_4}{2}\zeta_s + \Delta\right) + \tanh\frac{\beta}{2}\left(\frac{J_3}{2}\xi_{1s} - \frac{J_4}{2}\zeta_s - \Delta\right)\right],$$
$$\zeta_s = \frac{1}{2}\left[\tanh\frac{\beta}{2}\left(\frac{J_3}{2}\xi_{1s} + \frac{J_4}{2}\zeta_s + \Delta\right) - \tanh\frac{\beta}{2}\left(\frac{J_3}{2}\xi_{1s} - \frac{J_4}{2}\zeta_s - \Delta\right)\right]. \tag{2.14}$$

3. Thermodynamic characteristics of RHS

To calculate the dielectric, piezoelectric, and elastic characteristics RHS, we use the electric thermodynamical potential per unit cell obtained in the mean field approximation

$$\begin{aligned} g = \frac{G}{N} \;=\; & \nu U_{\text{seed}} - 4\frac{1}{\beta}\ln 2 - \frac{1}{\beta}\sum_{f=1}^{4}\ln\cosh\frac{\beta}{2}\mathscr{H}_f \\ & + \frac{1}{2}\Big(J_1^0 + \sum_{i=1}^{3}\bar{\psi_1}_i\varepsilon_i + \sum_{j=4}^{6}\bar{\psi_1}_j\varepsilon_j\Big)\xi_1^2 + \frac{1}{2}\Big(J_2^0 + \sum_{i=1}^{3}\bar{\psi}_{2i}\varepsilon_i + \sum_{j=4}^{6}\bar{\psi_2}_j\varepsilon_j\Big)\xi_2^2 \\ & + \frac{1}{2}\Big(J_3^0 + \sum_{i=1}^{3}\bar{\psi}_{3i}\varepsilon_i + \sum_{j=4}^{6}\bar{\psi_3}_j\varepsilon_j\Big)\xi_3^2 + \frac{1}{2}\Big(J_4^0 + \sum_{i=1}^{3}\bar{\psi}_{4i}\varepsilon_i + \sum_{j=4}^{6}\bar{\psi_4}_j\varepsilon_j\Big)\zeta^2. \end{aligned} \tag{3.1}$$

From the thermodynamic equilibrium conditions

$$\frac{1}{\nu}\left(\frac{\partial g}{\partial \varepsilon_i}\right)_{E_i} = 0, \qquad \frac{1}{\nu}\left(\frac{\partial g}{\partial \varepsilon_j}\right)_{E_i,\sigma_i} = 0, \qquad \frac{1}{\nu}\left(\frac{\partial g}{\partial E_i}\right) = -P_i$$

we obtain

$$
\begin{aligned}
0 &= c_{1i}^{E0}(T)\varepsilon_1 + c_{i2}^{E0}(T)\varepsilon_2 + c_{i3}^{E0}(T)\varepsilon_3 - e_{3i}^0 E_3 - \frac{\bar{\psi_{1i}}}{2\nu}\xi_1^2 - \frac{\bar{\psi_{2i}}}{2\nu}\xi_2^2 - \frac{\bar{\psi_{3i}}}{2\nu}\xi_3^2 - \frac{\bar{\psi_{4i}}}{2\nu}\zeta^2 - \frac{2\psi_{5i}}{\nu}\zeta,\\
0 &= c_{44}^{E0}(T)\varepsilon_4 - \frac{\bar{\psi_{14}}}{2\nu}\xi_1^2 - \frac{\bar{\psi_{24}}}{2\nu}\xi_2^2 - \frac{\bar{\psi_{34}}}{2\nu}\xi_3^2 - \frac{\bar{\psi_{44}}}{2\nu}\zeta^2 - \frac{2\psi_{54}}{\nu}\zeta,\\
0 &= c_{55}^{E0}(T)\varepsilon_5 - e_{35}^0 E_3 - \frac{\bar{\psi_{15}}}{2\nu}\xi_1^2 - \frac{\bar{\psi_{25}}}{2\nu}\xi_2^2 - \frac{\bar{\psi_{35}}}{2\nu}\xi_3^2 - \frac{\bar{\psi_{45}}}{2\nu}\zeta^2 - \frac{2\psi_{55}}{\nu}\zeta,\\
0 &= c_{66}^{E0}(T)\varepsilon_6 - \frac{\bar{\psi_{16}}}{2\nu}\xi_1^2 - \frac{\bar{\psi_{26}}}{2\nu}\xi_2^2 - \frac{\bar{\psi_{36}}}{2\nu}\xi_3^2 - \frac{\bar{\psi_{46}}}{2\nu}\zeta^2 - \frac{2\psi_{56}}{\nu}\zeta,\\
P_1 &= e_{11}^0\varepsilon_1 + e_{12}^0\varepsilon_2 + e_{13}^0\varepsilon_3 + e_{15}^0\varepsilon_5 + \chi_{11}^{\varepsilon 0}E_1 + \frac{2\mu_1}{\nu}\xi_1,\\
P_2 &= e_{24}^0\varepsilon_4 + e_{26}^0\varepsilon_6 + \chi_{22}^{\varepsilon 0}E_2 + \frac{2\mu_2}{\nu}\xi_2,\\
P_3 &= e_{31}^0\varepsilon_1 + e_{32}^0\varepsilon_2 + e_{33}^0\varepsilon_3 + e_{35}^0\varepsilon_5 + \chi_{33}^{\varepsilon 0}E_3 + \frac{2\mu_3}{\nu}\xi_3.
\end{aligned}
\tag{3.2}
$$

In the ferroelectric phase, the static isothermic dielectric permittivities of mechanically clamped RHS along the crystallographic axes are as follows:

$$
\chi_{iis}^{T\varepsilon}(0) = \lim_{E_i\to 0}\left(\frac{\partial P_i}{\partial E_i}\right)_{\varepsilon_j} = \chi_{ii}^{\varepsilon 0} + \frac{\mu_i^2}{\nu}\beta F_{1is}(0). \tag{3.3}
$$

The following notations are used

$$
\begin{aligned}
F_{11s}(0) &= \frac{\rho_{31} - (\rho_{31}^2 - \rho_{32}^2)\frac{\beta J_2}{4}}{1 - \rho_{31}\left(\frac{\beta J_1}{4} + \frac{\beta J_2}{4}\right) + (\rho_{31}^2 - \rho_{32}^2)\frac{\beta J_1}{4}\frac{\beta J_2}{4}},\\
F_{12s}(0) &= \frac{\rho_{31} - (\rho_{31}^2 - \rho_{32}^2)\frac{\beta J_1}{4}}{1 - \rho_{31}\left(\frac{\beta J_1}{4} + \frac{\beta J_2}{4}\right) + (\rho_{31}^2 - \rho_{32}^2)\frac{\beta J_1}{4}\frac{\beta J_2}{4}},\\
F_{13s}(0) &= \frac{\rho_{31} - (\rho_{31}^2 - \rho_{32}^2)\frac{\beta J_4}{4}}{1 - \rho_{31}\left(\frac{\beta J_3}{4} + \frac{\beta J_4}{4}\right) + (\rho_{31}^2 - \rho_{32}^2)\frac{\beta J_3}{4}\frac{\beta J_4}{4}},
\end{aligned}
$$

and

$$
\rho_{31} = 1 - \xi_{3s}^2 - \zeta_s^2, \qquad \rho_{32} = 2\xi_{3s}\zeta_s.
$$

In the paraelectric phase:

$$
\chi_{iip}^{T\varepsilon}(0) = \chi_{ii}^{\varepsilon 0} + \frac{\mu_i^2}{\nu}\beta F_{1ip}(0), \qquad (i = 1,2,3), \tag{3.4}
$$

where

$$
F_{1ip}(0) = \frac{1 - \zeta_p^2}{1 - (1 - \zeta_p^2)\frac{\beta J_i}{4}}.
$$

From relations (3.3), we get expressions for isothermic piezoelectric coefficients e_{ij} of RHS

$$
e_{3is}^T = \left(\frac{\partial P_3}{\partial \varepsilon_i}\right)_{E_3} = e_{3i}^0 + \frac{\mu_3}{\nu}\frac{\beta}{2}\left[\bar{\psi}_{3i}\xi_{3s}F_{13s}(0) - \left(\bar{\psi}_{4i}\zeta_s + 2\psi_{5i}\right)\bar{F}_{13s}(0)\right],
$$

$$
e_{35s}^T = \left(\frac{\partial P_3}{\partial \varepsilon_5}\right)_{E_3} = e_{35}^0 + \frac{\mu_3}{\nu}\frac{\beta}{2}\left[\bar{\psi}_{35}\xi_{3s}F_{13s}(0) - \left(\bar{\psi}_{45}\zeta_s + 2\psi_{55}\right)\bar{F}_{13s}(0)\right].
$$

By differentiating the relations (3.3) with respect to the strains at a constant polarization, we obtain the expressions for the for piezoelectric constants

$$
h_{3is}^T = \frac{e_{3is}}{\chi_{33s}^{\varepsilon}}, \qquad h_{35s}^T = \frac{e_{35s}}{\chi_{33s}^{\varepsilon}}. \tag{3.5}
$$

Now, we calculate the contributions of the pseudospin system to the elastic constants of RHS. From (3.2) we obtain the relations for elastic coefficients at a constant field:

$$\begin{aligned} c^{TE}_{ii's} &= \left(\frac{\partial\sigma_i}{\partial\varepsilon_{i'}}\right)_{E_i} = c^{E0}_{ii'}(T) - \frac{\beta\bar{\psi_{3i}}\bar{\psi_{3i'}}}{4\upsilon}\xi^2_{3s}F_{13s}(0) - \frac{\beta\left(\bar{\psi_{4i}}\zeta_s + 2\psi_{5i}\right)\left(\bar{\psi_{4i'}}\zeta_s + 2\psi_{5i'}\right)}{4\upsilon}F_{14s}(0) \\ &\quad + \frac{\beta\left(\bar{\psi_{3i}}\bar{\psi_{4i'}} + \bar{\psi_{3i'}}\bar{\psi_{4i}}\right)}{4\upsilon}\xi_{3s}\zeta_s\bar{F}_{13s}(0) + \frac{\beta\left(\bar{\psi_{4i}}\psi_{5i'} + \bar{\psi_{4i'}}\psi_{5i}\right)}{2\upsilon}\xi_{3s}\bar{F}_{13s}(0), \quad (3.6) \\ c^{TE}_{ii'p} &= c^{E0}_{ii'}(T) - \frac{\beta\left(\bar{\psi_{4i}}\zeta_p + 2\psi_{5i}\right)\left(\bar{\psi_{4i'}}\zeta_p + 2\psi_{5i'}\right)}{4\upsilon}F_{14p}(0), \\ c^{TE}_{jjs} &= \left(\frac{\partial\sigma_j}{\partial\varepsilon_j}\right)_{E_i} = c^{E0}_{jj}(T) - \frac{\beta\bar{\psi^2_{3j}}}{4\upsilon}\xi^2_{3s}F_{13s}(0) - \frac{\beta\left(\bar{\psi_{4j}}\zeta_s + 2\psi_{5j}\right)^2}{4\upsilon}F_{14s}(0) \\ &\quad + \frac{\beta\bar{\psi_{3j}}\bar{\psi_{4j}}}{2\upsilon}\xi_{3s}\zeta_s\bar{F}_{13s}(0) + \frac{\beta\bar{\psi_{3j}}\psi_{5j}}{\upsilon}\xi_{3s}\bar{F}_{13s}(0), \quad (3.7) \\ c^{TE}_{jjp} &= c^{E0}_{jj}(T) - \frac{\beta\left(\bar{\psi_{4j}}\zeta_s + 2\psi_{5j}\right)^2}{4\upsilon}F_{14p}(0), \end{aligned}$$

where

$$F_{14s}(0) = \frac{\rho_{31} - (\rho^2_{31} - \rho^2_{32})\frac{\beta J_3}{4}}{1 - \rho_{31}(\frac{\beta J_3}{4} + \frac{\beta J_4}{4}) + (\rho^2_{31} - \rho^2_{32})\frac{\beta J_3}{4}\frac{\beta J_4}{4}}, \qquad F_{14p}(0) = \frac{1-\zeta^2_p}{1-(1-\zeta^2_p)\frac{\beta J_4}{4}}.$$

From (3.2), (3.3) we get isothermic coefficients of piezoelectric strain $d_{1i} = (\partial P_1/\partial\sigma_i)_{E_1}$, $d_{ij} = (\partial P_i/\partial\sigma_j)_{E_i}$ in the following form:

$$d^T_{3i} = \sum_{k=1}^{3} s^{TE}_{ik}e^T_{3k} + s^{TE}_{i5}e^T_{35}, \qquad d^T_{35} = s^{TE}_{15}e^T_{31} + s^{TE}_{25}e^T_{32} + s^{TE}_{35}e^T_{33} + s^{TE}_{55}e^T_{35},$$

where $s^E_{ik} = (\partial\varepsilon_i/\partial\sigma_k)_{E_1}$, $s^E_{jj} = (\partial\varepsilon_j/\partial\sigma_j)_{E_i}$ are the compliances at the constant field.

Using relations (3.3) one can obtain the expression for the static dielectric permittivity of a free RHS crystal

$$\chi^{T\sigma}_{33} = \left(\frac{\partial P_3}{\partial E_3}\right)_{\sigma_6} = \chi^{T\varepsilon}_{23} + e^T_{31}d^T_{31} + e^T_{32}d^T_{32} + e^T_{33}d^T_{33} + e^T_{35}d^T_{35}.$$

Molar entropy of RHS caused by its pseudospin subsystem is as follows:

$$S = -R\left(\frac{\partial g}{\partial T}\right) = R\Big[4\ln 2 + \sum_{f=1}^{4}\ln\cosh\frac{\beta}{2}\mathscr{H}_f - 2\gamma_1\xi_1 - 2\gamma_2\xi_2 - 2\gamma_3\xi_3 - 2\delta\varsigma\Big], \quad (3.8)$$

where R is the universal gas constant. Molar heat capacity at a constant pressure is calculated by differentiating the entropy (3.8)

$$\Delta C^\sigma = T\left(\frac{\partial S}{\partial T}\right)_\sigma. \quad (3.9)$$

4. Relaxation dynamics of RHS crystal

This section describes the dynamic phenomena in RHS at the application of electrical field E^*_1 to a crystal. While calculating the dynamic characteristics, we use the kinetic equation [25, 26] based on the Zubarev nonequilibrium statistical operator method [27].

The kinetic equation for the mean values of pseudospin operator is as follows:

$$\frac{\mathrm{d}}{\mathrm{d}t}\langle\hat{p}_m\rangle = -\sum_{qf}\sum_{\mu\alpha}\left[Q^-_{qf\mu\alpha}(\hat{p}_m) + \tanh\frac{\beta\Omega^\alpha_\mu}{2}Q^+_{qf\mu\alpha}(\hat{p}_m)\right]K^\alpha_\mu, \quad (4.1)$$

where

$$Q^{\mp}_{qf\mu\alpha}(\hat{p}_m) = \langle\Big[\big[\hat{p}_m, \sigma^{-\alpha}_{qf}\big(\Omega^{\alpha'}_{\mu}\big)\big], \sigma^{\alpha}_{qf}\big(\Omega^{\alpha}_{\mu}\big)\Big]^{\mp}\rangle_q, \tag{4.2}$$

$$K^{\alpha}_{\mu} = \int_0^{\infty} \mathrm{d}t \mathrm{e}^{-\varepsilon t} \cos\Omega^{\alpha}_{\mu} t \mathrm{Re}\langle\bar{u}(t)\bar{u}^{+}\rangle_q, \qquad \alpha = 0, \pm 1, \tag{4.3}$$

while $\langle\bar{u}^{\alpha}(t)\bar{u}^{\alpha'}\rangle_q$ is correlation function of the thermostat; $\sigma^{\alpha}_{qf}\big(\Omega^{\alpha}_{\mu}\big)$ is a Fourier component of the operator $\sigma^{\alpha}_{qf}(t)$; Ω^{α}_{μ} are the eigenfrequencies of the Hamiltonian of the quasispin model (2.6); $\sigma^{0}_{qf} = \sigma_{qf}$, $\sigma^{\pm}_{qf} = \sigma^{x}_{qf} \pm i\sigma^{y}_{qf}$.

Taking into account (2.7), operators $\hat{p}_m$ have such a form:

$$\hat{P}_m = \frac{\sigma_{qf}}{2}. \tag{4.4}$$

Using the evolution law of the quasispin operators S^{α}_{qf} ($\alpha = 0\pm$) and their permutation relations, we calculate the commutators occurring in (4.2) as well as the expression for $Q^{\mp}_{qf\mu\alpha}(\hat{p}_m)$. The kinetic equation (4.1) can be rewritten as follows:

$$-\frac{\mathrm{d}}{\mathrm{d}t}\eta_f = 2K_f\eta_f - 2K_f \tanh\frac{\beta H_f}{2}, \tag{4.5}$$

where

$$K_f = \int_0^{\infty} \mathrm{d}t \mathrm{e}^{-\varepsilon t} \cos(H_f t) \mathrm{Re}[\langle\bar{u}^{-}(t)\bar{u}^{+}\rangle_q + \langle\bar{u}^{+}(t)\bar{u}^{-}\rangle_q].$$

Note that at $K_f = \frac{1}{2\alpha}$, the obtained kinetic equation (4.5) agrees with the equation found within the stochastic Glauber model [28]. Using the variables $\xi_1, \xi_2, \xi_3, \zeta$ in equations (4.5), we obtain

$$\begin{aligned}
-\alpha\frac{\mathrm{d}}{\mathrm{d}t}\xi_1 &= \xi_1 - \frac{1}{4}(-L_1 - L_2 + L_3 + L_4),\\
-\alpha\frac{\mathrm{d}}{\mathrm{d}t}\xi_2 &= \xi_2 - \frac{1}{4}(-L_1 - L_2 - L_3 - L_4),\\
-\alpha\frac{\mathrm{d}}{\mathrm{d}t}\xi_3 &= \xi_3 - \frac{1}{4}(L_1 + L_2 + L_3 + L_4),\\
-\alpha\frac{\mathrm{d}}{\mathrm{d}t}\zeta &= \zeta - \frac{1}{4}(L_1 - L_2 + L_3 - L_4),
\end{aligned} \tag{4.6}$$

where the following notations are used:

$$\begin{aligned}
L_1 &= \tanh\frac{1}{2}(-\gamma_1 - \gamma_2 + \gamma_3 + \delta), & L_2 &= \tanh\frac{1}{2}(-\gamma_1 + \gamma_2 + \gamma_3 - \delta),\\
L_3 &= \tanh\frac{1}{2}(\gamma_1 + \gamma_2 + \gamma_3 + \delta), & L_4 &= \tanh\frac{1}{2}(\gamma_1 - \gamma_2 + \gamma_3 - \delta).
\end{aligned} \tag{4.7}$$

The dynamic properties RHS are explored using the system of equations (4.6) and at small deviations from the equilibrium. We separate these equations into the static and dynamic parts. The distribution functions are presented as sums of two components: the equilibrium functions and their deviations from the equilibrium values (fluctuations)

$$\xi_1 = \tilde{\xi}_1 + \xi_{it}, \qquad (i = 1,2,3), \qquad \zeta = \tilde{\zeta} + \zeta_t. \tag{4.8}$$

Also $E_{it} = E_{i0}\mathrm{e}^{\mathrm{i}\omega t}$.

As a result, we obtain the following system of equations for the fluctuation parts:

$$-\frac{\mathrm{d}}{\mathrm{d}t}\begin{pmatrix}\xi_{1ts}(1)\\ \xi_{2ts}(1)\end{pmatrix} = \begin{pmatrix}a_{11} & a_{12}\\ a_{21} & a_{22}\end{pmatrix}\begin{pmatrix}\xi_{1ts}(1)\\ \xi_{2ts}(1)\end{pmatrix} - \frac{\beta\mu_1 E_{1t}}{2}\begin{pmatrix}a_1\\ a_2\end{pmatrix}, \tag{4.9}$$

$$-\frac{\mathrm{d}}{\mathrm{d}t}\begin{pmatrix}\xi_{2ts}(2)\\ \xi_{1ts}(2)\end{pmatrix}=\begin{pmatrix}b_{11} & b_{12}\\ b_{21} & b_{22}\end{pmatrix}\begin{pmatrix}\xi_{2ts}(2)\\ \xi_{1ts}(2)\end{pmatrix}-\frac{\beta\mu_2 E_{2t}}{2}\begin{pmatrix}b_1\\ b_2\end{pmatrix}, \tag{4.10}$$

$$-\frac{\mathrm{d}}{\mathrm{d}t}\begin{pmatrix}\xi_{3ts}(3)\\ \zeta_{st}(3)\end{pmatrix}=\begin{pmatrix}c_{11} & c_{12}\\ c_{21} & c_{22}\end{pmatrix}\begin{pmatrix}\xi_{3ts}(3)\\ \zeta_{st}(3)\end{pmatrix}-\frac{\beta\mu_3 E_{3t}}{2}\begin{pmatrix}c_1\\ c_2\end{pmatrix}. \tag{4.11}$$

Solving the systems (4.9)–(4.11), we find the dynamic permittivities of the clamped RHS crystal

$$\varepsilon^{\varepsilon}_{iis}(\omega)=\varepsilon^{\varepsilon 0}_{iis}+\sum_{j=1}^{2}\frac{4\pi\chi_{jis}}{1+(\omega\tau_{jis})^2}+i\sum_{j=1}^{2}\frac{4\pi\omega\tau_{jis}\chi_{jis}}{1+(\omega\tau_{jis})^2}. \tag{4.12}$$

In (4.12)

$$\chi_{1is}=\frac{\mu_i^2}{v}\beta\frac{\tau_{1is}\tau_{2is}}{\tau_{1is}-\tau_{2is}}\Big[-m^{(1)}(i)+\tau_{1is}m^{(0)}(i)\Big],\qquad \chi_{2is}=\frac{\mu_i^2}{v}\beta\frac{\tau_{1is}\tau_{2is}}{\tau_{1is}-\tau_{2is}}\Big[m^{(1)}(i)-\tau_{2is}m^{(0)}(i)\Big],$$

$$\tau^{-1}_{\substack{1\\2}is}=\frac{1}{2}\Big[m_1(i)\mp\sqrt{m_1^2(i)-4m_0(i)}\Big]. \tag{4.13}$$

In (4.13), we use the following notations:

$$\begin{aligned}
&m_1(1)=m_1(2)=\frac{1}{\alpha}\left(1-\rho_{31}\frac{\beta J_1}{4}\right)+\frac{1}{\alpha}\left(1-\rho_{31}\frac{\beta J_2}{4}\right),\\
&m_0(1)=m_0(2)=\frac{1}{\alpha^2}\left[1-\rho_{31}\left(\frac{\beta J_1}{4}+\frac{\beta J_2}{4}\right)+\left(\rho_{31}^2-\rho_{32}^2\right)\frac{\beta J_1}{4}\frac{\beta J_2}{4}\right],\\
&m^{(0)}(1)=\frac{1}{\alpha^2}\left[\rho_{31}-\left(\rho_{31}^2-\rho_{32}^2\right)\frac{\beta J_2}{4}\right],\qquad m^{(0)}(2)=\frac{1}{\alpha^2}\left[\rho_{31}-\left(\rho_{31}^2-\rho_{32}^2\right)\frac{\beta J_1}{4}\right].\\
&m_1(3)=\frac{1}{\alpha}\left(1-\rho_{31}\frac{\beta J_3}{4}\right)+\frac{1}{\alpha}\left(1-\rho_{31}\frac{\beta J_4}{4}\right),\\
&m_0(3)=\frac{1}{\alpha^2}\left[1-\rho_{31}\left(\frac{\beta J_3}{4}+\frac{\beta J_4}{4}\right)+\left(\rho_{31}^2-\rho_{32}^2\right)\frac{\beta J_3}{4}\frac{\beta J_4}{4}\right],\\
&m^{(1)}(3)=\frac{1}{\alpha}\rho_{31},\qquad m^{(0)}(3)=\frac{1}{\alpha^2}\left[\rho_{31}-\left(\rho_{31}^2-\rho_{32}^2\right)\frac{\beta J_4}{4}\right].
\end{aligned}$$

5. Comparison of numerical results with experimental data

To compare the temperature and field dependences of the above derived dielectric, piezoelectric, elastic, and thermal characteristics of RHS, we need to set the values of the following parameters: the interaction potentials J^0, K^0_{12}, K^0_{13}, K^0_{14} and, accordingly, J_1, J_2, J_3, J_4; the parameter Δ, which characterizes an asymmetry of populations of the two equilibrium positions of a dipole; the deformation potentials ψ_{ij}; effective dipole moments μ_i; seed dielectric permittivities $\chi^{\varepsilon 0}_{ii}$; piezoelectric coefficients e^0_{ij}; elastic constants $c^{E0}_{ii'}$ and c^{E0}_{jj}, and the parameter α that defines the time scale of the relaxation processes.

To find the optimum values of the theory parameters it is necessary to use the dependence of temperature T_{c} on hydrostatic pressure. Unfortunately, different sources give different values for $T_{\mathrm{c}}(0)$, varying from 258 K to 265.1 K. We shall use $T_{\mathrm{c}}(0)=265$ K [14].

In the fitting procedure, we use the experimentally obtained values for the temperature dependences of the following physical characteristics of RHS: $P_s(T)$ [20], $\varepsilon^{\sigma}_{11}(0)$, $\varepsilon^{\sigma}_{22}(0)$ [23], $\varepsilon_{33}(\omega)$ [14], as well as the dependence $T_{\mathrm{c}}(p)$ [29] of the transition temperature on hydrostatic pressure. In the case of deuterted RDS crystal, we exploit $P_s(T)$ [16], $\varepsilon^{\sigma}_{33}(0)$ [16], $T_{\mathrm{c}}(p)$ [29].

In order to find the values of the parameters $J^0+K^0_{13}$, $K^0_{12}+K^0_{14}$, Δ, we found the point at the phase diagram (a,b), where

$$a=\frac{(J^0+K^0_{13})-(K^0_{12}+K^0_{14})}{(J^0+K^0_{13})+(K^0_{12}+K^0_{14})},\qquad b=\frac{\Delta}{(J^0+K^0_{13})+(K^0_{12}+K^0_{14})},$$

at which the system undergoes a single second order phase transition at $T_c(0) = 265$ K. The values of the effective dipole moments μ_3 were determined by fitting the calculated spontaneous polarization to experiment.

The values of J^0, K^0_{12}, K^0_{13}, K^0_{14}, μ_1, and μ_2 are determined by fitting the calculated ε_{11} and ε_{22} to the experimental data given in [23].

The fitting procedure for the models of this class is described in detail in [30], where the thermodynamic characteristics of Rochelle salt are explored.

The strains should be taken into account in order to calculate the dielectric permittivity of a mechanically free crystal, piezoelectric coefficients, and elastic constants. Therefore, to determine the values of the deformation potentials ψ_{ij}, we analyzed their effect on theoretical values of physical characteristics of the crystal. Thus, it has been obtained that an increase of the transition temperature with hydrostatic pressure [29] can be described using the values of ψ_{ij} presented here. It should be stressed that when the piezoelectric coefficients are measured experimentally, the values of ψ_{ij} can be determined with a greater accuracy.

The parameter α_H is determined from the condition that the theoretically calculated frequency dependences of $\varepsilon_{33}(\omega)$ agree with the experiment. We also assume that the parameter α_H is a weak function of temperature:

$$\alpha_H = [P_H + R_H(\Delta T)] \times 10^{-14}, \qquad \Delta T = T - T_c.$$

The unit cell volume of RHS is $v = 0.842 \cdot 10^{-21}$ cm^3.

The obtained sets of optimal parameters are given in table 1.

Table 1. The optimal sets of the theory parameters for $Rb(H_{1-x}D_x)SO_4$.

x	J^0/k_B K	K^0_{12}/k_B K	K^0_{13}/k_B K	K^0_{14}/k_B K	Δ/k_B K	μ_1, 10^{-18} esu·cm	μ_2, 10^{-18} esu·cm	μ_3, 10^{-18} esu·cm	$\chi^{\varepsilon 0}_{11}$	$\chi^{\varepsilon 0}_{22}$	$\chi^{\varepsilon 0}_{33}$
0.0	394	190	372	433.7	244	3.18	3.65	0.81	0.02	0.02	0.159
0.7	380	189	345	430.8	245			0.90	0.02	0.02	0.159
1.0	378	198.8	338.4	429	245.4			1.00	0.02	0.02	0.159

x	P_{3s} (s)	R_{3s} (s/K)	P_{3p} (s)	P_{3p} (s/K)	$P_{1,2}$ (s)	$R_{1,2}$ (s/K)
0.0	12.5	–0.0521	12.5	–0.091	10.5	–0.001
0.7	10.7	–0.0510	10.7	–0.051		
1.0	9.8	–0.0510	9.8	–0.0501		

The deformation potentials are taken to be $\bar{\psi}_{1i}/k_B = \bar{\psi}_{1j}/k_B = \bar{\psi}_{2i}/k_B = \bar{\psi}_{2j}/k_B = 900$ K, $\bar{\psi}_{31}/k_B = -4950$ K, $\bar{\psi}_{32}/k_B = \bar{\psi}_{33}/k_B = \bar{\psi}_{35}/k_B = -4500$ K, $\bar{\psi}_{41}/k_B = 1080$ K, $\bar{\psi}_{42}/k_B = \bar{\psi}_{43}/k_B = \bar{\psi}_{45}/k_B = 900$ K, $\bar{\psi}_{51}/k_B = \bar{\psi}_{52}/k_B = \bar{\psi}_{53}/k_B = \bar{\psi}_{55}/k_B = 200$ K.

The "seed" constants for RHS are $e^0_{31} = e^0_{32} = e^0_{33} = e^0_{35} = -1 \times 10^4$ esu/cm^2, $c^{0E}_{11} = 32.0 \times 10^{10}$ dyn/cm^2, $c^{E0}_{12} = 17.0 \times 10^{10}$ dyn/cm^2, $c^{E0}_{13} = 8.7 \times 10^{10}$ dyn/cm^2, $c^{E0}_{22} = 38 \times 10^{10}$ dyn/cm^2, $c^{E0}_{23} = 6.5 \times 10^{10}$ dyn/cm^2, $c^{E0}_{33} = 37.4 \times 10^{10}$ dyn/cm^2, $c^{E0}_{44} = 4.9 \times 10^{10}$ dyn/cm^2, $c^{E0}_{55} = 5.3 \times 10^{10}$ dyn/cm^2, $c^{E0}_{66} = 12.8 \times 10^{10}$ dyn/cm^2; $k_{11} = -0.032 \times 10^{10}$ dyn/(cm^{2}K), $k_{12} = -0.040 \times 10^{10}$ dyn/(cm^{2}K), $k_{13} = -0.015 \times 10^{10}$ dyn/(cm^{2}K), $k_{23} = -0.010 \times 10^{10}$ dyn/(cm^{2}K) $k_{33} = -0.032 \times 10^{10}$ dyn/(cm^{2}K), $k_{22} = k_{44} = k_{55}$=0.0. We use the same values for RDS as well.

Now we discuss the obtained results. In figure 2, the temperature dependences of the strains ε_i and ε_j are presented. In the ferroelectric phase, ε_i slightly increases with temperature, while the temperature variation of ε_4, ε_6, and especially ε_5 is much stronger. In the paraelectric phase, all these strains weakly increase with temperature. The temperature dependences of spontaneous polarization P_s of RHS and RDS along with the experimentally obtained values [16, 17, 20] are shown in figure 3. A good description of experimental data of [20] and [16] is reached. When the deuteration level x increases, the polarization decreases.

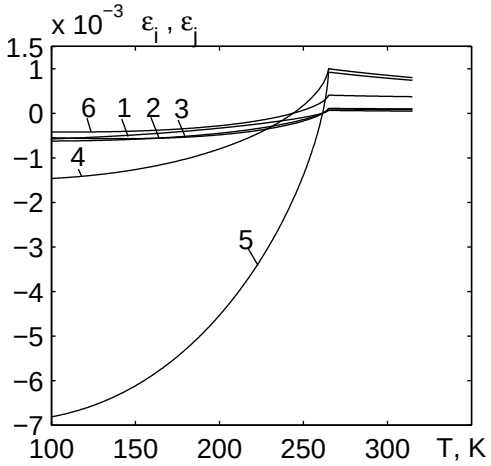

Figure 2. The temperature dependences of the strains ε_i and ε_j of RHS: ε_1 — 1, ε_2 — 2, ε_3 — 3,ε_4 — 4, ε_5 — 5 i ε_6 — 6.

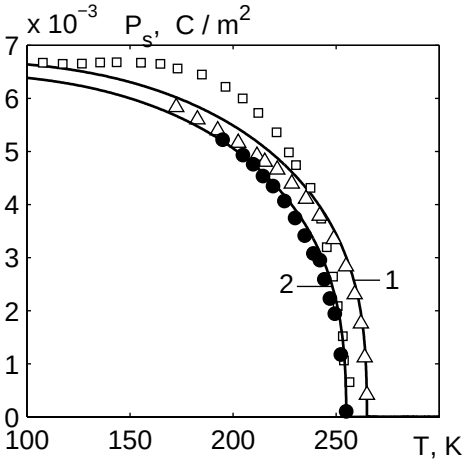

Figure 3. The temperature dependences of spontaneous polarization of RHS — 1, △ [20], □ [17] and RDS — 2, • [16].

Figure 4 shows the calculated temperature dependences of static dielectric permittivities of the mechanically clamped $\varepsilon_{33}^{\varepsilon}(0,T)$ and free $\varepsilon_{33}^{\sigma}(0,T)$ RHS crystal along with the experimental data [17, 19, 20, 23].

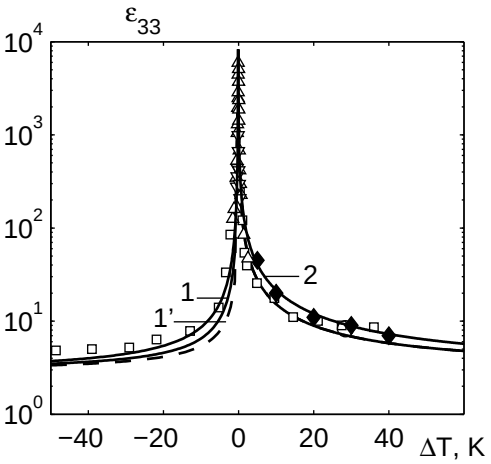

Figure 4. The temperature dependences of static dielectric permittivities of RHS, 1 — $\varepsilon_{33}^{\sigma}$, 1' — $\varepsilon_{33}^{\varepsilon}$, ▽ [19], △ [20], □ [17], ○ [23] and RDS — 2, ♦ [16].

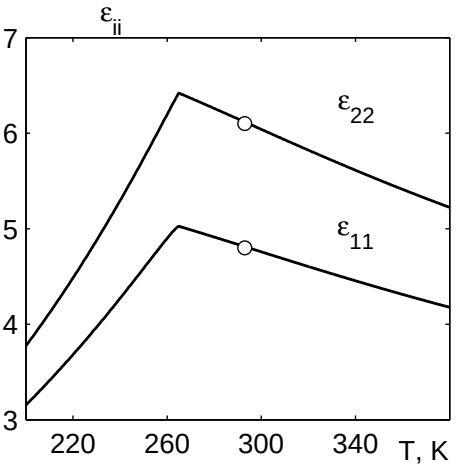

Figure 5. The temperature dependences of the transverse permittivities ε_{11} and ε_{22} of RHS. ○ [23].

The permittivity $\varepsilon_{33}^{\sigma}(0,T)$ is larger than $\varepsilon_{33}^{\varepsilon}(0,T)$. An increase of deuteron concentration increases the permittivity $\varepsilon_{33}^{\varepsilon}(0,T)$ at all temperatures. As shown in figure 4, the theoretical results $\varepsilon_{33}^{\sigma}(0,T)$ are in a good quantitative agreement with experimental data of [17, 19, 20, 23]. At temperature $T = T_c$, the value of the permittivity $\varepsilon_{33}^{\sigma}(0,T)$ is very large, which is typical of the second order phase transitions.

Figure 5 illustrates the temperature dependences of the transverse permittivities ε_{11} and ε_{22} of a RHS crystal. They are significantly smaller than the longitudinal permittivity.

The temperature dependences of piezoelectric coefficients e_{3i} and e_{55} and constants h_{3i} and h_{35} are given in figure 6. In the paraelectric phase, these coefficients are equal to zero, whereas in the ferroelectric phase, e_{3i} and e_{55} values have a deep minimum at approaching T_c, and h_{31}, h_{35} constants change insignificantly.

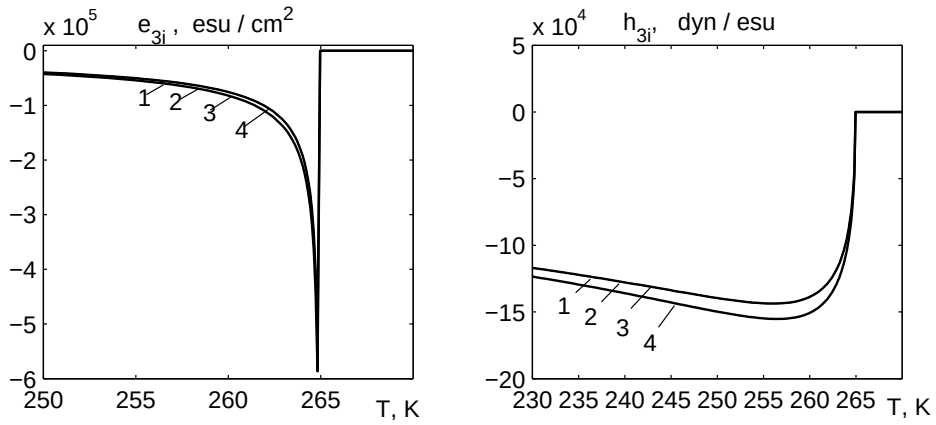

Figure 6. The temperature dependences of piezoelectric coefficients e_{31} —1, e_{32} —2, e_{33} —3, e_{35} —4 and constants h_{31} —1, h_{32} —2, h_{33} —3, h_{35} —4 of RHS.

In figure 7 we show the temperature dependences of the elastic constants c_{ij}^E. A good description of experimental data [23] is obtained, except for the temperature dependence of elastic constants c_{12}^E, c_{22}^E, and c_{23}^E in the ferroelectric phase, for which the experimental measurements predict deep minima near T_c.

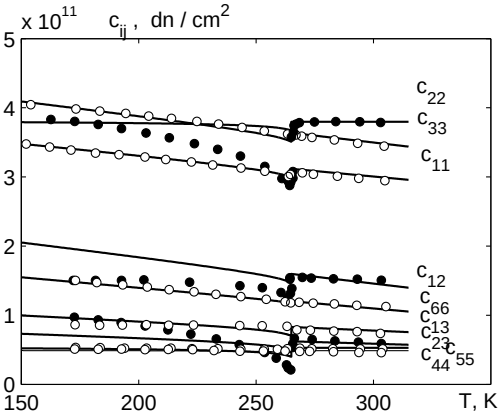

Figure 7. The temperature dependences of the elastic constants c_{ij}^E of RHS, ∘ — [23], lines: the theory.

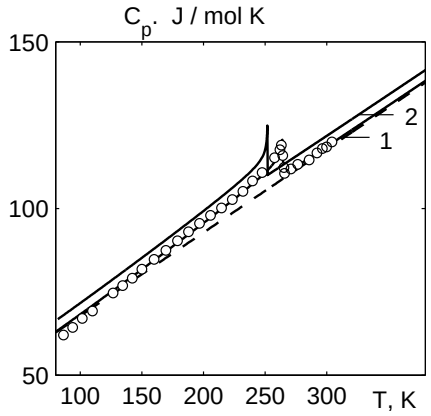

Figure 8. The temperature dependences of heat capacity of RHS — 1, • [31] and RDS — 2.

The temperature dependences of heat capacity of RHS and RDS crystals along with experimental data [31] are depicted in figure 8.

By a dashed line we show the effective lattice heat capacity contribution C_0, which we estimate as an average difference $C_{\exp}(T) - \Delta C(T)$. A quantitatively good description of experiment [31] is obtained. The calculated value of the heat capacity jump is also in a good agreement with experiment. Deuteration increases the heat capacity in the entire temperature range.

Figures 9–11 show the temperature dependences of the real $\varepsilon_{33}^{\varepsilon'}(\nu, T)$ and imaginary $\varepsilon_{33}^{\varepsilon''}(\nu, T)$ parts of the dynamic dielectric permittivity at different frequencies and compositions of partially deuterated $Rb(H_{1-x}D_x)SO_4$ crystals (at $x = 0.0, 0.70, 1.00$) along with the experimental data [14, 32, 35].

As seen in the figures, the proposed model yields a good description of experimental data for the $Rb(H_{1-x}D_x)SO_4$ crystals over a wide temperature range at different frequencies. For all frequencies, at $\Delta T = 0$ K, the dynamic permittivity $\varepsilon_{33}'(\nu, T)$ has a sharp minimum, where the permittivity values drop to $\varepsilon_{33}^{0\varepsilon}$; the minimum width increases with an increasing frequency. The maximum in the temperature curve of $\varepsilon_{33}'(\nu, T)$ above T_c lowers down, smears out, and shifts to higher temperatures at an increasing

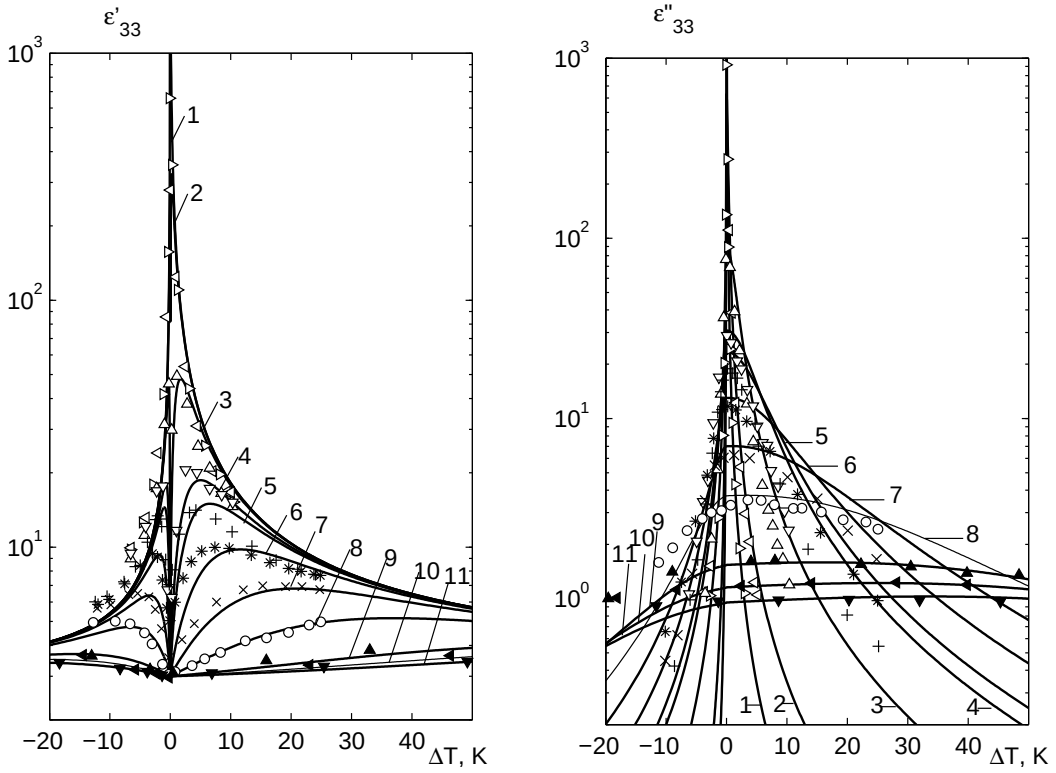

Figure 9. The temperature dependences of the real $\varepsilon_{33}^{\varepsilon'}(\nu, T)$ and imaginary $\varepsilon_{33}^{\varepsilon''}(\nu, T)$ parts of the dynamic dielectric permittivity of RHS at different frequencies ν (GHz): 0.150 — 1, ▷ [32]; 0.455 — 2, ◁ [32]; 3.27 — 3, △ [32]; 9.50 — 4, ▽ [32], 8.72 — 5, + [14]; 12.5 — 6, ∗ [14]; 22.5 — 7, × [14]; 41.7 — 8, ○ [14]; 190 — 9, ▲ [35]; 253 — 10, ◀ [35]; 307 — 11, ▼ [35].

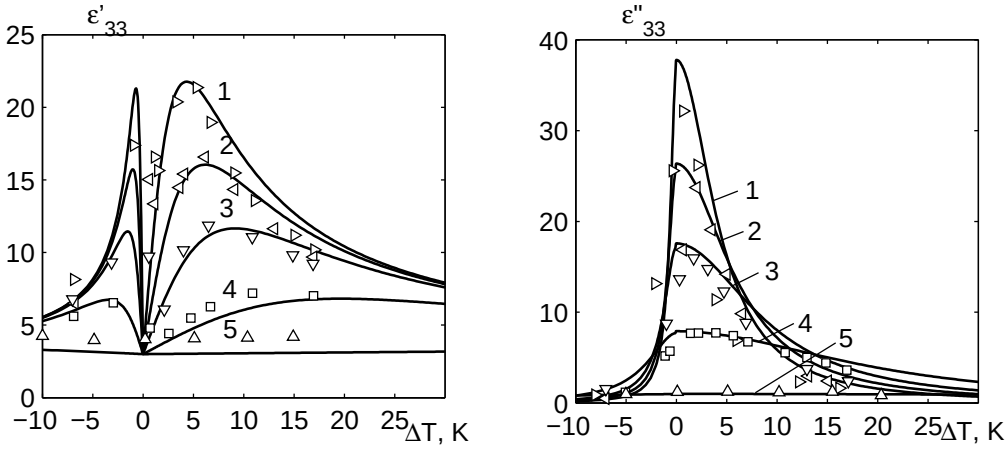

Figure 10. The temperature dependences of the real ε'_{33} and imaginary ε''_{33} parts of the dynamic dielectric permittivity of $Rb(H_{0.30}D_{0.70})SO_4$ at different frequencies ν (GHz): 8.72 — 1, ▷ [14]; 12.5 — 2, ◁ [14]; 18.72 — 3, ▽ [14]; 41.70 — 4, □ [14]; 330 — 5, △ [14].

frequency. The dispersion width of the real part of the permittivity in the paraelectric phase is wider than in the ferroelectric phase.

In figures 12 and 13, we plot the temperature dependences of the real and imaginary parts of the transverse dielectric permittivities ε'_{11}, ε''_{11} and ε'_{22}, ε''_{22} of RHS at different frequencies.

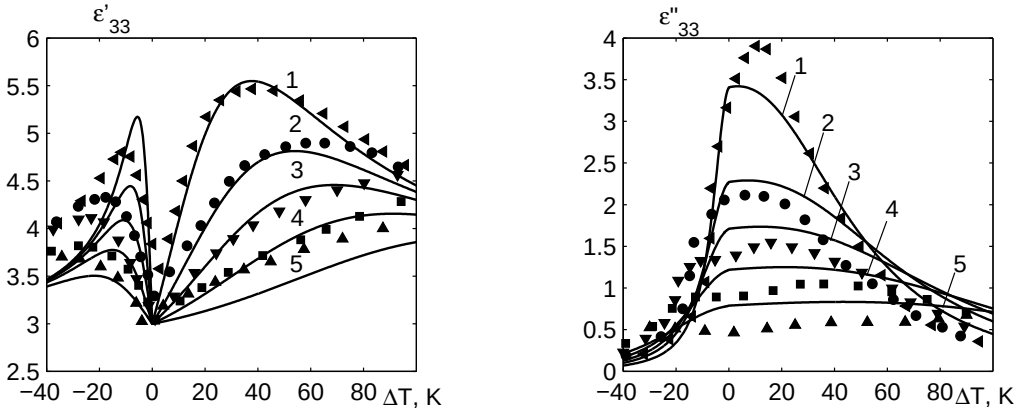

Figure 11. The temperature dependences of the real ε'_{33} and imaginary ε''_{33} parts of the dynamic dielectric permittivity of RDS at different frequencies ν (GHz): 118 — 1, ◅ [35]; 177 — 2, • [35]; 235 — 3, ▼ [35]; 330 — 4, ■ [35]; 510 — 5, ▲ [35].

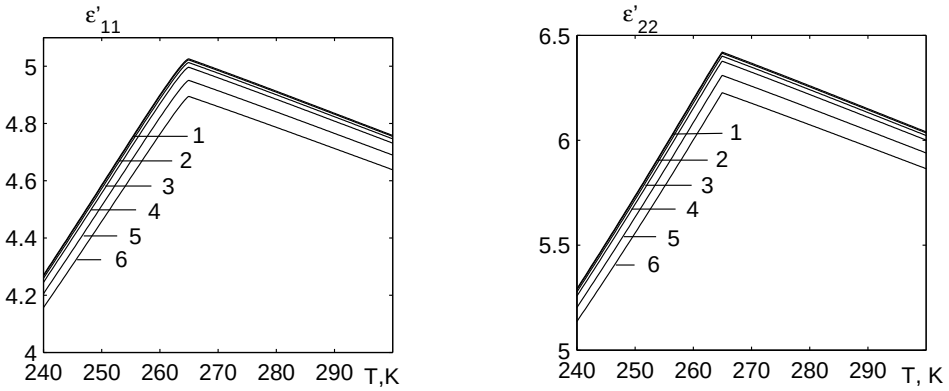

Figure 12. The temperature dependences of the real ε'_{11} and ε'_{22} parts of the dynamic dielectric permittivity of RDS at different frequencies ν (GHz): 0 — 1; 41.7 — 2; 78.5 — 3; 118 — 4; 190 — 5; 253 — 6.

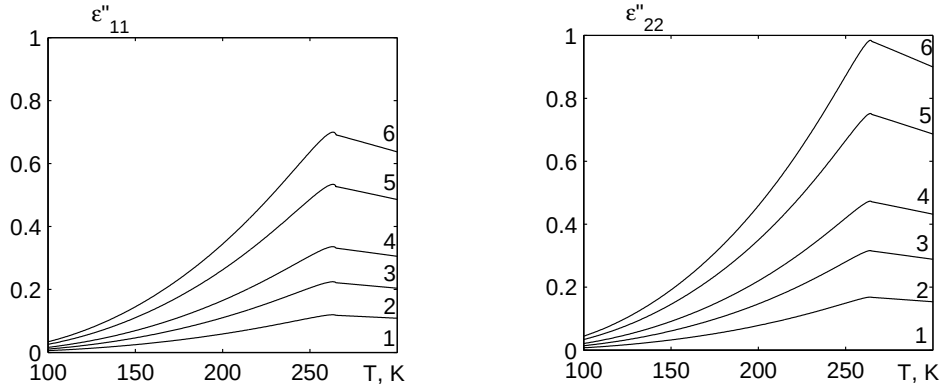

Figure 13. The temperature dependences of the imaginary ε''_{11} and ε''_{22} parts of the dynamic dielectric permittivity of RDS at different frequencies ν (GHz): 0 — 1; 41.7 — 2; 78.5 — 3; 118 — 4; 190 — 5; 253 — 6.

In figure 14, we plot the calculated frequency dependences of $\varepsilon'_{33}(\nu)$ and $\varepsilon''_{33}(\nu)$ for RHS at different temperatures $\Delta T = 2$, 5, 10, 20 K and in figure 15 for $Rb(H_{1-x}D_x)_2SO_4$ with $x = 0.70$ along with the experimental points.

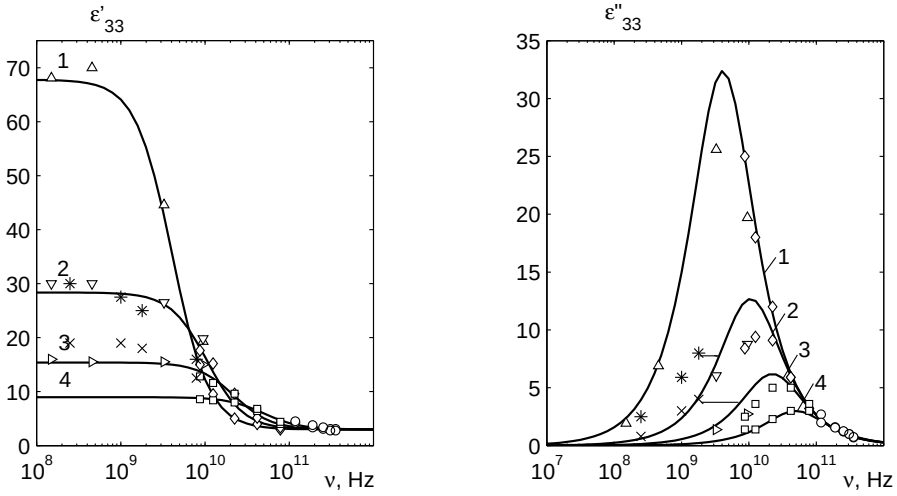

Figure 14. The frequency dependences of $\varepsilon'_{33}(\nu)$ and $\varepsilon''_{33}(\nu)$ for RHS at ΔT: 2 — 1; 5 — 2; 10 — 3; 20 — 4. $\triangle$ [32]; $\bullet$ [33]; $\circ$ [14]; $\square$ [35], $\times, *$ [33].

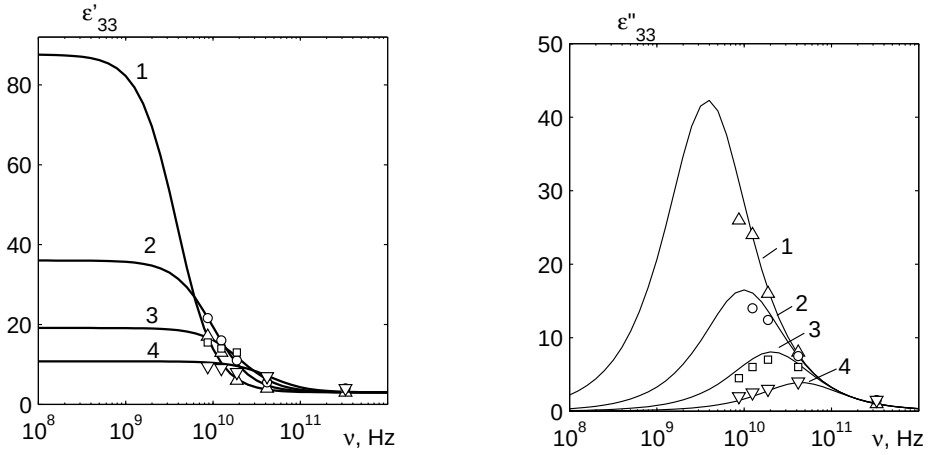

Figure 15. The frequency dependences of $\varepsilon'_{33}(\nu)$ and $\varepsilon''_{33}(\nu)$ for $Rb(H_{1-x}D_x)_2SO_4$ at $x = 0.70$ at ΔT: 2 — 1, $\triangle$ [14]; 5 — 2, $\circ$ [14]; 10 — 3, $\square$ [14]; 20 — 4, $\triangledown$ [14].

As one can see, the theory is in a good agreement with experiment, except for the data of [33] where the permittivity dispersion was observed at frequencies lower than in [14, 32, 35]. When ΔT increases, the dispersion of $\varepsilon_{33}(\nu, T)$ shifts to higher frequencies.

6. Conclusions

In this paper, using the modified four-sublattice model of a $RbHSO_4$ crystal, with taking into account the piezoelectric coupling to the ε_i, ε_j strains, within the framework of the mean field approach, the theory of the thermodynamic, dielectric, piezoelectric, elastic, and dynamic properties of RHS crystals has been developed. A thorough numerical analysis of the dependences of the calculated characteristics on the model parameters has been performed. Optimal sets of these parameters and "seed" characteristics for RHS crystals have been found which enabled us to describe the available experimental data.

References

1. Nelmes R.J., Ferroelectrics, 1972, **4**, 133; doi:10.1080/00150197208235754.
2. Ashmore J.P., Petch H.E., Can. J. Phys., 1975, **53**, 2694; doi:10.1139/p75-328.
3. Iton K., Ohno H., Kuragaki S., J. Phys. Soc. Jpn., 1995, **64**, 479; doi:10.1143/JPSJ.64.479.
4. Iton K., Moriyoshi C., Ferroelectrics, 2003, **285**, 91; doi:10.1080/00150190390205933.
5. Kasahara M., Tatsuzaki I., J. Phys. Soc. Jpn., 1974, **36**, 786; doi:10.1143/JPSJ.36.786.
6. Kasahara M., Tatsuzaki I., J. Phys. Soc. Jpn., 1974, **37**, 167; doi:10.1143/JPSJ.37.167.
7. Kasahara M., Tatsuzaki I., J. Phys. Soc. Jpn., 1975, **38**, 1389; doi:10.1143/JPSJ.38.1389.
8. Mjasnikova E.P., Yacenko A.F., Fiz. Tverd. Tela, 1962, **4**, 653 (in Russian).
9. Bazhulyn P.A., Mjasnikova E.P., Rarov A.V., Fiz. Tverd. Tela, 1963, **5**, 1784 (in Russian).
10. Nakamura E., Kajikawa H., J. Phys. Soc. Jpn., 1978, **44**, 519; doi:10.1143/JPSJ.44.519.
11. Blat D.H., Zinenko V.I., Fiz. Tverd. Tela, 1976, **18**, 3588 (in Russian).
12. Levitsky R.R., Zachek I.R., Varanisky V.I., Fiz. Tverd. Tela, 1980, **22**, 2750 (in Russian).
13. Paprotny W., Grigas J., Levitsky R.R., Kutny I.V., Krasikov V.S., Ferroelectrics, 1984, **61**, 19; doi:10.1080/00150198408018932.
14. Grigas J., Zacekas I., Krasikovas V., Kutnas I., Levickis R., Paprotnas V., Lietuvos Fizikos Rinkinys, 1984, **24**, No. 6, 33.
15. Levitsky R.R., Andrusyk A.Ya., Preprint of the Institute for Condensed Matter Physics, ICMP-11-03U, Lviv, 2011 (in Ukrainian).
16. Ichikawa M., J. Phys. Soc. Jpn., 1979, **47**, 1562; doi:10.1143/JPSJ.47.1562.
17. Pepinsky R., Vedam K., Phys. Rev., 1960, **117**, No. 3, 1502; doi:10.1103/PhysRev.117.1502.
18. Nakamura E., Kajikawa H., Ozaki T., J. Phys. Soc. Jpn., 1977, **42**, 1427; doi:10.1143/JPSJ.42.1427.
19. Flerov I.N., Iskornev I.M., Fiz. Tverd. Tela, 1976, **18**, 3666 (in Russian).
20. Kajikawa H., Ozaki T., Nakamura E., J. Phys. Soc. Jpn., 1977, **43**, 937; doi:10.1143/JPSJ.43.937.
21. Stasyuk I.V., Levitsky R.R., Moina A.P., Slivka O.G., Velychko O.V., Field and Deformational Effects in Complex Ferroelectric Compounds, Grazhda, Uzhgorod, 2009 (in Ukrainian).
22. Stasyuk I., Velychko O., Ferroelectrics, 2005, **316**, 51; doi:10.1080/00150190590963138.
23. Zajceva M.P., Shabanova L.A., Zherebcova L.I., Fiz. Tverd. Tela, 1979, **21**, 2308 (in Russian).
24. Levitsky R.R., Lisnii B.M., Phys. Status Solidi B, 2004, **241**, 1350; doi:10.1002/pssb.200301995.
25. Berim G.O., Kessel A.R., Physica A, 1980, **101**, No. 1, 112; doi:10.1016/0378-4371(80)90103-X.
26. Berim G.O., Kessel A.R., Physica A, 1980, **101**, No. 1, 127; doi:10.1016/0378-4371(80)90104-1.
27. Zubarev D.N., Noneguilibrium Statistical Thermodynamics, Consultants Bureau, New York, 1974.
28. Glauber J., J. Math. Phys., 1963, **4**, No. 2, 294; doi:10.1063/1.1703954.
29. Gesi K., Ozawa K., J. Phys. Soc. Jpn., 1975, **38**, 459; doi:10.1143/JPSJ.38.459.
30. Levitsky R.R., Zachek I.R., Vdovych A.S., Stasyuk I.V., Condens. Matter Phys., 2009, **12**, No. 2, 295; doi:10.5488/CMP.12.2.295.
31. Alexanrov K.S., Anistratov A.T., Blat D.X., Zherebtsova L.I., Zinenko V.I., Iskornev I.M., Melnikova S.V., Flerov I.N., Kirenski L.V., Ferroelectrics, 1976, **12**, 191; doi:10.1080/00150197608241423.
32. Ozaki T., J. Phys. Soc. Jpn., 1980, **49**, 234; doi:10.1143/JPSJ.49.234.
33. Krasikov V.S., Ushatkin K.F., Ogurcov C.V., Fiz. Tverd. Tela, 1979, **21**, 617 (in Russian).
34. Krasikov V.S., Ogurcov C.V., Ushatkin K.F., Fiz. Tverd. Tela, 1981, **23**, 3425 (in Russian).
35. Ambrazjavichene V.S., Volkov A.A., Kozlov G.V., Krasikov V.S., Krjukova E.B., Fiz. Tverd. Tela, 1983, **25**, 1605 (in Russian).

Статистична теорія термодинамічних та динамічних властивостей сегнетоелектрика $RbHSO_4$

І.Р. Зачек[1], Р.Р. Левицький[2], Я.Й. Щур[2], О.Б. Біленька[1]

[1] Національний університет "Львівська політехніка", вул. С. Бандери, 12, 79013 Львів, Україна

[2] Інститут фізики конденсованих систем НАН України, вул. І. Свєнціцького, 1, 79011 Львів, Україна

Використовуючи модифіковану чотирипідграткову модель $RbHSO_4$ шляхом врахування п'єзоелектричного зв'язку з деформаціями ε_i, ε_4, ε_5 і ε_6, в наближенні молекулярного поля розраховано компоненти вектора поляризації та тензора статичної діелектричної проникності механічно затиснутого і вільного кристалів, їх п'єзоелектричні характеристики і пружні сталі. Розраховано також динамічні проникності механічно затиснутого кристалу $RbHSO_4$. При знайденому наборі параметрів теорії отримано для цих характеристик задовільний кількісний опис наявних експериментальних даних.

Ключові слова: *сегнетоелектрики, діелектрична проникність, п'єзомодулі*

PACS: *77.22.Ch, 77.22.Gm, 77.65.-j, 77.80.Bh, 77.84.-s*